Energetics in Correlation with Structural Features: The Case of Micellization

Jurij Lah,* Marija Bešter-Rogač,* Tine-Martin Perger, and Gorazd Vesnaver

Faculty of Chemistry and Chemical Technology, University of Ljubljana, Aškerčeva 5, 1000 Ljubljana, Slovenia

Received: May 8, 2006; In Final Form: September 1, 2006

Understanding micellization processes at the molecular level has direct relevance for biological self-assembly, folding, and association processes. As such, it requires complete characterization of the micellization thermodynamics, including its correlation with the corresponding structural features. In this context, micellization of a series of model non-ionic surfactants (poly(ethylene glycol) monooctyl ethers, C_8E_Y) was studied by isothermal titration calorimetry (ITC) and differential scanning calorimetry (DSC). The corresponding structural properties of C_8E_Y micelles were investigated by small-angle X-ray scattering (SAXS). The C_8E_Y micellization, characterized independently from ITC, DSC, and structural data, reveals that $\Delta H_M^\circ > 0$, $\Delta S_M^\circ > 0$, and $\Delta C_{P,M}^\circ < 0$, while the dissection of its energetics shows that it is primarily governed by the transfer of 20−30 C_8 alkyl chains from aqueous solution into the nonpolar core ($r \approx 1.3$ nm) of the spherical micelle. Moreover, thermodynamic parameters of micellization, estimated from the structural features related to the changes in solvent-accessible surface areas upon micellization, are in a good agreement with the corresponding parameters obtained from the analysis of ITC and DSC data. We have shown that the contributions to ΔS_M° other than from hydration ($\Delta S_{M,other}^\circ$), estimated from experimental data, appear to be small ($\Delta S_{M,other}^\circ < 0.1\Delta S_M^\circ$) and agree well with the theoretical estimates expressed as a sum of the corresponding translational, conformational, and size contributions. These $\Delta S_{M,other}^\circ$ contributions are much less unfavorable than those estimated for a rigid-body association, which indicates the dynamic nature of the C_8E_Y micellar aggregates.

Introduction

When protein or nucleic acid molecules fold, when ligands bind to macromolecules, when drugs enter biomembranes, or when surfactant molecules micellize, the interacting sites on individual amino acids, nucleotides, or other molecules are removed from water to come into contact with each other. The apparent disaffinity of water for the nonpolar (interacting) surfaces, known as the hydrophobic effect, has been widely studied because it plays a key role in these and many other chemical and biological processes.[1−11] Owing to the structural complexity of biological macromolecules, model compounds have often been employed to characterize thermodynamically the hydrophobic effect as one of the main driving forces of folding and binding processes.[9−26] Numerous experiments measuring the partitioning of model compounds between a pure organic phase and water suggest that the thermodynamic parameters describing their transfer from one phase into the other may be expressed as a sum of contributions of constituent groups that make up the compound.[26−35] This property, known as group additivity, allows one to dissect the observed thermodynamic parameters into the contributions that arise from the hydrophobic effect and other fundamental interactions. Such approach, often successfully used for predicting energetics of protein folding and protein−protein association from the relevant structural data, is based on the dissection of thermodynamic parameters that follows from the estimated changes in the solvent-accessible nonpolar (ΔA_N) and polar (ΔA_P) surface areas of the solute and the accompanying changes in the conformational, translational, and rotational entropy.[30,36−45]

There is no doubt that understanding micelle formation at the molecular level has direct relevance for biological self-assembly processes, folding of membrane proteins, protein−protein interactions in biological membranes, etc., as well as for many industrial applications.[1,46−51] The micellization process itself and the properties of micelles in solution have been widely studied[1,52−54] by means of experimental thermodynamics,[54−78] structure,[79−88] and theory.[89−117] However, no general relations connecting Gibbs free energy (ΔG_M°), enthalpy (ΔH_M°), entropy (ΔS_M°), and heat capacity ($\Delta C_{P,M}^\circ$) of micellization with the micelles' structural properties have been established. The question we are trying to answer in this work is whether the approach that has been successfully applied for correlating structural and thermodynamic characteristics of protein folding and protein−protein association[26,27,39−44] is general enough to be used also in characterization of micellization processes. In other words, can we use this approach to estimate micellar structural features from the thermodynamic parameters of micellization and vice versa? To investigate this question, we studied micellization of a series of model non-ionic surfactants (poly(ethylene glycol) monooctyl ethers, C_8E_Y) in aqueous solutions.

Generally speaking, the most suitable method for determining the basic thermodynamic properties of a given process is calorimetry, because it is the only method that measures directly the true, model-independent enthalpy changes. Isothermal titration calorimetry (ITC) measures the concentration dependence of heat effects at a constant temperature and has been frequently used in quantitative thermodynamic studies of micellization.[62−66,69−78,118] In contrast, corresponding studies of the temperature dependence of the excess heat capacity at a fixed concentration by differential scanning calorimetry (DSC)

* Corresponding authors. J.L.: phone +386 1 2419 414, fax +386 1 2419 425, E-mail jurij.lah@fkkt.uni-lj.si. M.B.-R.: phone +386 1 2419 410, fax +386 1 2419 425, E-mail marija.bester@fkkt.uni-lj.si.

10.1021/jp062796f CCC: $33.50
Published on Web 10/26/2006

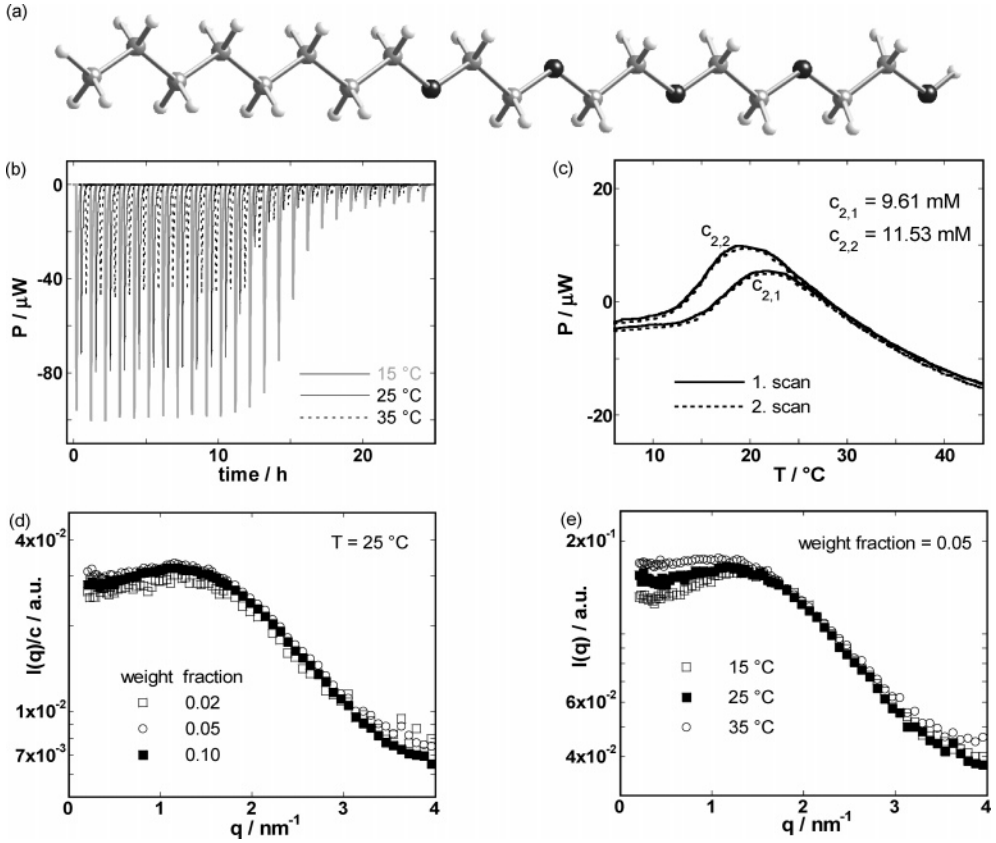

Figure 1. (a) Schematic representation of a C_8E_Y molecule (carbon, dark gray; oxygen, black; hydrogen, light gray). (b,c) Typical raw ITC and DSC signals resulting from demicellization−micellization of C_8E_4. (d,e) Typical SAXS signals of the C_8E_4 micellar solutions (eq 2).

are rather scarce.[74,119] By employing these two methods, we would like to answer the following questions: (i) Can we use DSC as an independent method for the determination of $\Delta G_M°$, $\Delta H_M°$, $\Delta S_M°$, $\Delta C_{P,M}°$, and the micellar aggregation number, n? (ii) What are the limitations of ITC and DSC for studying micellization? (iii) Can we use thermodynamic parameters of micellization obtained by ITC and DSC to estimate the corresponding ΔA_N and ΔA_P values?

Another possibility is to obtain ΔA_N and ΔA_P from the structural features. However, in this case, the structures of the final (micelle) and the initial states (monomers) have to be defined. For micellization this seems to be more difficult than in the case of conformational transitions and association processes involving proteins, nucleic acids, and small molecules, where for at least one macro state (folded, bound) structures are often known (X-ray, NMR), and thus their solvent-accessible surface areas can be calculated using the well-known methods described elswhere.[33,120,121] In an attempt to estimate ΔA_N, ΔA_P, and the corresponding thermodynamic parameters of micellization from the structural features, we used the information obtained from small-angle X-ray scattering measurements, supported by the corresponding theoretical analysis. This approach enables us to correlate thermodynamics of micellization with the corresponding structural features at a number of levels, since the thermodynamic parameters, the populations of surfactant molecules existing in the monomeric and micellar macro states, the relative partition functions, and the corresponding accessible surface areas can be estimated using thermodynamic and structure-based calculations.

To the best of our knowledge, the work presented here is the first complete thermodynamic study of micellization in which the observed thermodynamic quantities of micellization are discussed in terms of various contributions arising from the solute−solute, solute−solvent, and solvent−solvent interactions and correlated to the measured micellar structural features.

Materials and Methods

Surfactants. Tetraethylene glycol monooctyl ether (C_8E_4), pentaethylene glycol monooctyl ether (C_8E_5), and hexaethylene glycol monooctyl ether (C_8E_6), purchased from Anatrace, Inc. (Maumee, OH) as 50% water solutions (purity >99%), were used as received. The C_8E_Y molecule is presented schematically in Figure 1a.

Isothermal Titration Calorimetry (ITC). In a typical demicellization experiment, the heat effects resulting from mixing aliquots of titrant solution, injected by a motor-driven syringe, with the solution (solvent) in the titration cell were measured using a TAM 2277 calorimeter (Thermometric, Stockholm, Sweden) (Figure 1). Two milliliters of degassed, triple-distilled water was titrated at several temperatures between 15 and 45 °C by a degassed surfactant solution placed in a 250 μL syringe. Surfactant concentrations in the syringe were 0.30−0.36 M. Before each experiment, the instrument was calibrated by means of a known electric pulse. The area under the peak following each injection of the surfactant solution, obtained by integration of the raw signal (Figure 1b), is proportional to the heat effect expressed per mole of added surfactant per injection. By subtracting heat effects that accompany or would accompany (extrapolation) complete demicellization of the added surfactant from the measured heat effects, the corresponding ΔH versus c_2 curve (Figure 2a,b) was constructed.

Differential Scanning Calorimetry (DSC). DSC was performed with a Nano-II differential scanning calorimeter (CSC, Lindon, UT). After degassing (15 min) of surfactant solutions (7−12 mM), at least two consecutive scans were performed at

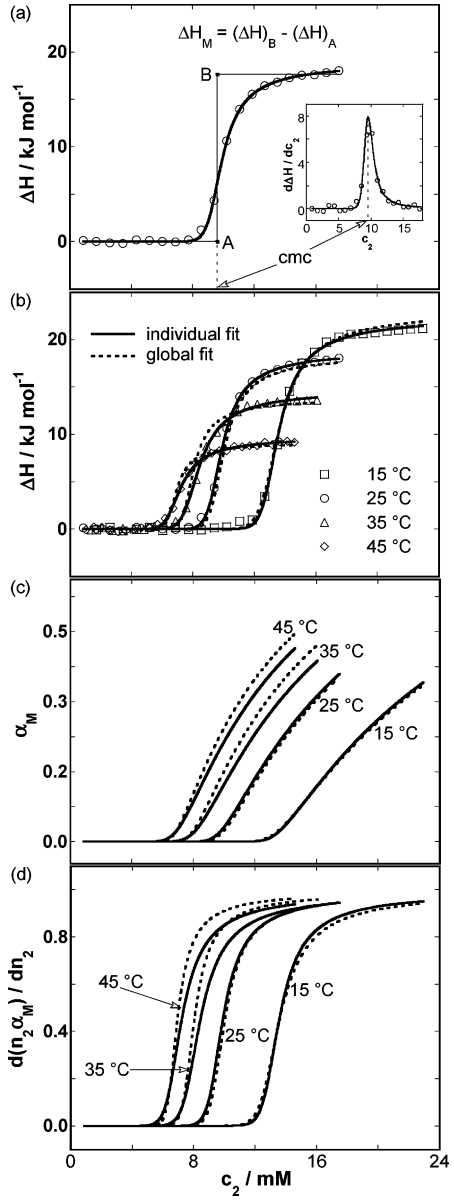

Figure 2. Model analysis of ITC signals accompanying demicellization of C_8E_5. (a) Determination of enthalpy of micellization, ΔH_M, by pseudo-phase separation model. Inset: cmc determined according to Philips's criterion. Symbols are experimental points, while the full line represents the best fit of the reversible two-state model (rts; see eqs 5, 7−10). (b) The best (individual) fits of the rts model to the ITC curves at a given temperature (full lines) and the corresponding global rts model fit to the family of the ITC curves measured at different temperatures (disconnected lines; the best-fit global parameters are $n = 28$, $\Delta G_M°(T_o) = -10.5$ kJ mol^{-1}, $\Delta H_M°(T_o) = 18.6$ kJ mol^{-1}, and $\Delta C_{P,M}° = -0.46$ kJ mol^{-1} K^{-1} at $T_o = 25$ °C). Experimental points are presented as symbols. (c,d) The fraction of surfactant molecules in the micellar form, α_M, and the $(\partial(n_2\alpha_M)/\partial n_2)_{n_1,P,T}$ derivative (n_2 is the total amount of surfactant monomers in the solution) as functions of the total surfactant concentration in the measuring cell, c_2, that result from individual and global rts analysis.

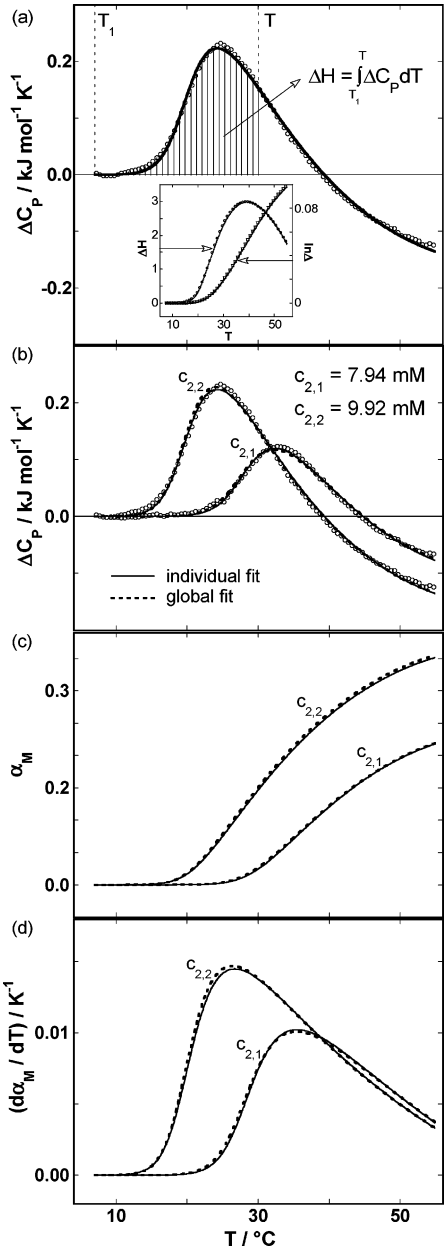

Figure 3. Model analysis of DSC thermograms accompanying micellization of C_8E_5. (a) The best fits (lines) of the reversible two-state model (rts; eqs 6, 7−9, 11) to the corresponding experimental heat capacity, ΔC_P (every fifth experimental point is presented as a symbol). Inset: The corresponding enthalpy of transition, ΔH, and logarithm of partition function, ln Δ, as functions of temperature. (b) The best (individual) fits of the rts model to the DSC curves at a given concentration (full lines) and the corresponding global rts fit to the family of the DSC curves measured at different concentrations (disconnected lines; the best-fit global parameters are $n = 22$, $\Delta G_M°(T_o) = -10.5$ kJ mol^{-1}, $\Delta H_M°(T_o) = 17.7$ kJ mol^{-1}, and $\Delta C_{P,M}° = -0.43$ kJ mol^{-1} K^{-1} at $T_o = 25$ °C). Experimental points are presented as symbols. (c,d) The fraction of surfactant molecules in the micellar form, α_M, and its temperature derivative as functions of temperature, resulting from individual and global rts analysis.

a heating rate of 1 °C min^{-1}. For each surfactant, measurements were performed in the range from 0 °C to the phase separation temperature (about 47 °C for C_8E_4, 66 °C for C_8E_5, and 68 °C for C_8E_6; see Supporting Information), where the observed transitions appear to be reversible. Thermograms, ΔC_P versus T (Figure 3a,b), were obtained from the raw signals (Figure 1c), corrected for the solvent contribution (baseline) by subtracting the corresponding heat capacity of the initial (monomeric) surfactant state extrapolated along the whole measured temperature range. The corresponding model-independent transition enthalpies, ΔH, were calculated as the areas under the ΔC_P versus T curves (Figure 3a).

Small-Angle X-ray Scattering (SAXS). SAXS measurements were performed with an evacuated Kratky compact camera system (Anton Paar, Graz, Austria) with a block collimating unit, attached to a conventional X-ray generator (Bruker AXS, Karlsruhe, Germany) equipped with a sealed

X-ray tube (Cu-anode target type), producing Ni-filtered Cu K_α X-rays with a wavenlength of 0.154 nm. The tube was operating at 35 kV and 35 mA. The samples were transferred to a standard quartz capillary placed in a thermally controlled sample holder, centered in the X-ray beam. The scattering intensities were measured with a linear, position-sensitive detector (PSD 50m, M. Braun, Garsching, Germany), detecting the scattering pattern within the whole scattering range simultaneously. All measurements were performed in the temperature range between 15 and 45 °C. For each sample, five SAXS curves with a sampling time of 15 000 s were recorded and subsequently averaged to ensure reliable statistics, smoothed, and corrected for solvent scattering. The absorption of the solutions was determined by using the "moving slit" method.[122]

The smeared data were corrected for experimental broadening by numerical de-smearing based on the measured beam cross-section profiles. The result of these calculations is a desmeared scattering function and the pair-distance distribution function $p(r)$,

$$p(r) = \frac{1}{2\pi^2}\int_0^\infty I(q)(qr)\sin(qr)\,\mathrm{d}q \qquad (1)$$

which is the Fourier transform of the scattering function,[123]

$$I(q) = 4\pi\int_0^\infty p(r)\frac{\sin(qr)}{qr}\,\mathrm{d}r \qquad (2)$$

where q is a scattering vector, defined as $q = (4\pi/\lambda)\sin(\theta/2)$, λ is the wavelength of X-rays, θ is the scattering angle between the incident beam and the scattered radiation, and r is the distance between two scattering centers within the particle. $p(r)$ was evaluated from the measured $I(q)$ using the indirect Fourier transformation method (program ITP).[124,125] For spherical symmetry, $p(r)$ simplifies to $p(r) = r^2\Delta\tilde{\rho}^2(r)$, where $\Delta\tilde{\rho}^2(r)$ is the spatially averaged autocorrelation function (convolution square) of the electron density fluctuations, given by the general expression

$$\Delta\tilde{\rho}^2(r) = \langle\Delta\tilde{\rho}^2(r)\rangle = \left\langle\int_{-\infty}^{+\infty}\Delta\rho(\mathbf{r}_1)\Delta\rho(\mathbf{r}_1-\mathbf{r})\,\mathrm{d}r_1\right\rangle \qquad (3)$$

in which $\Delta\rho(\mathbf{r})$ represents the local scattering contrast, that is, the difference between the local scattering particle's electron density, $\rho(\mathbf{r})$, and the average electron density of the sample, $\bar{\rho}$. The scattering contrast profile, $\Delta\rho(\mathbf{r})$, of the scattering particles, which provides valuable information on the internal structure of scattering particles, can be calculated from the $p(r)$ function by a convolution square-root operation utilizing the DECON program.[126−129]

Thermodynamic Analysis

Analysis of Calorimetric Signals. In our calorimetric experiments, the measured solution in the calorimetric cell consisted of two components: solvent, 1 (water), characterized by the amount, n_1, and the partial molar enthalpy, $\bar{H}_1$, and solute, 2 (surfactant), characterized by the amount of surfactant, n_2, and the partial molar enthalpy of surfactant, $\bar{H}_2$. According to the two-state model, surfactant molecules are assumed to populate two thermodynamic (macro) states: monomeric state S, characterized by n_S (amount of monomers) and $\bar{H}_S$ (partial molar enthalpy of monomeric surfactant), and micellar state M, characterized by n_M (amount of monomers in the micellar form) and $\bar{H}_M$ (partial molar enthalpy of the surfactant in the micellar form). The enthalpy H of the solution in the calorimetric cell can be expressed at given P, T, and composition as

$$H = n_1\bar{H}_1 + n_2\bar{H}_2 = n_1\bar{H}_1 + n_S\bar{H}_S + n_M\bar{H}_M \qquad (4)$$

Recently, we have shown that, in ITC experiments (P, T = const.), the enthalpy changes accompanying injections of surfactant solution into the solution in the measuring cell can be expressed as $\bar{H}_2$ + const. (see Supporting Information).[118] Since, for the two-state model of micellization, $\bar{H}_2$ can also be derived by partial differentiation of eq 4 with respect to n_2 at constant P, T, and n_1, one obtains that, in combination with the Gibbs−Duhem equation, the corresponding measured relative partial molar enthalpy, ΔH (Figure 2a,b), may be expressed as

$$\Delta H = \bar{H}_2 - \bar{H}_S = \Delta H_M\left[\frac{\partial(n_2\alpha_M)}{\partial n_2}\right]_{n_1,P,T} = \Delta H_M^\circ\left[\frac{\partial(n_2\alpha_M)}{\partial n_2}\right]_{n_1,P,T} \qquad (5)$$

where $\alpha_M = n_M/n_2$ is the fraction of surfactant in the micellar form and the enthalpy of micelle formation, $\Delta H_M = \bar{H}_M - \bar{H}_S$, is defined as the enthalpy change accompanying the transition of 1 mol of surfactant monomers from the unaggregated form in the solution into the micellar form. The model function for describing the ITC data (right-hand side of eq 5) was obtained by assuming that ΔH_M is independent of concentration and thus equal to its value in the standard state ($\Delta H_M = \Delta H_M^\circ$).

In the DSC experiments (P, n_1, and n_2 = const.), the directly measured heat flow can be expressed in terms of the partial molar heat capacity of the solute, $\bar{C}_{P,2}$. Moreover, $\bar{C}_{P,2}$ can be obtained for the two-state model by taking the temperature derivative of eq 4 at constant P, n_1, and n_2 (see Supporting Information). Thus, the corresponding relative partial molar heat capacity of surfactant, normalized to zero micellization, ΔC_P (Figure 3a,b), may be expressed in terms of an appropriate model function that assumes concentration independence of enthalpy, ΔH_M, and heat capacity, $\Delta C_{P,M}$, of micellization ($\Delta H_M = \Delta H_M^\circ$ and $\Delta C_{P,M} = \Delta C_{P,M}^\circ$) as[130,131]

$$\Delta C_P = \bar{C}_{P,2} - \bar{C}_{P,S} = \Delta C_{P,M}^\circ\alpha_M + \Delta H_M^\circ\left[\frac{\partial\alpha_M}{\partial T}\right]_{n_1,n_2,P} \qquad (6)$$

where $\bar{C}_{P,S}$ is the partial molar heat capacity of surfactant in its monomeric form and $\Delta C_{P,M}^\circ = \bar{C}_{P,M} - \bar{C}_{P,S}$ is assumed to be independent of temperature. The experimental ΔH accompanying the temperature-induced micellization may be obtained by integration of ΔC_P (left side of eq 6) from the reference temperature, T_1, at which all surfactant molecules exist in the (monomeric) macro state S ($\alpha_M = 0$), to a given T at which a certain fraction of surfactant molecules exist in the micellar form (Figure 3a). The corresponding model ΔH is obtained by integration of the model function (right side of eq 6) within the same limits, which gives $\Delta H = \Delta H_M^\circ\alpha_M$ (note that both α_M and ΔH_M° are temperature dependent; Figure 3a). At this point, it should be mentioned that, according to the two-state model, one can describe the studied micellization process in the most general form in terms of the corresponding relative partition function Δ:[132] $\ln\Delta = \int_{T_1}^{T}[\Delta H/RT^2]\,\mathrm{d}T = \int_{T_1}^{T}[\Delta H_M^\circ\alpha_M/RT^2]\,\mathrm{d}T$.

In the analysis of ITC and DSC data, we used the integrated Gibbs−Helmholtz equation,

$$\Delta G_M^\circ = T\{\Delta G_M^\circ(T_o)/T_o + \Delta H_M^\circ(T_o)[1/T - 1/T_o] + \Delta C_{P,M}^\circ[1 - T_o/T - \ln(T/T_o)]\} \quad (7)$$

in which ΔG_M° is the standard Gibbs free energy of micellization at temperature T, $\Delta G_M^\circ(T_o)$ is the corresponding standard Gibbs free energy at some reference temperature T_o, and $\Delta H_M^\circ(T_o)$ is the standard enthalpy of micellization at T_o. To describe the measured ITC (eq 5) and DSC (eq 6) signals, the concentration and temperature dependence of α_M have to be specified. According to the reversible two-state (rts) model of micellization, which assumes that S and M forms are in equilibrium at any total molar concentration c_2, the micellization of the model surfactants at a given T may be described as

$$S \overset{K_M}{\longleftrightarrow} (1/n)M$$

$$\Delta G_M^\circ = -RT \ln K_M = -(RT/n) \ln\left(\frac{\alpha_M}{(1-\alpha_M)^n n c_2^{\,n-1}}\right) \quad (8)$$

In eq 8, n represents the micellar aggregation number and K_M the corresponding apparent equilibrium constant. According to the model (eq 8), the derivatives in eqs 5 and 6 may be expressed as

$$\left[\frac{\partial(n_2\alpha_M)}{\partial n_2}\right]_{n_1,P,T} = \frac{n\alpha_M}{1+(n-1)\alpha_M} \quad \text{and} \quad \left[\frac{\partial\alpha_M}{\partial T}\right]_{n_1,n_2,P} = \frac{\Delta H_M^\circ}{RT^2}\frac{n\alpha_M(1-\alpha_M)}{1+(n-1)\alpha_M} \quad (9)$$

Since $\Delta H_M^\circ = \Delta H_M^\circ(T_o) + \Delta C_{P,M}^\circ(T - T_o)$, it follows from eqs 5−9 that the ITC (eq 5) and DSC (eq 6) model functions may be, at any T and c_2, described only in terms of the parameters n, $\Delta G_M^\circ(T_o)$, $\Delta H_M^\circ(T_o)$, and $\Delta C_{P,M}^\circ$. Their values can be obtained by fitting the model function (ITC = eq 5, DSC = eq 6) to the experimental ITC (Figure 2a,b) or DSC (Figure 3a,b) data using the Levenberg−Marquardt nonlinear χ^2 regression procedure[133] and then further used to calculate the corresponding ΔG_M°, ΔH_M°, $T\Delta S_M^\circ$, α_M, and ln Δ quantities at some other temperature (Figures 5 and 7). However, the very high reciprocal correlation between parameters n and $\Delta G_M^\circ(T_o)$ observed in the analysis of ITC and DSC data suggests that the exact physical meaning of n and $\Delta G_M^\circ(T_o)$ may be questionable when both of them are used as adjustable parameters. This means that $\Delta G_M^\circ(T_o)$ and n values obtained from the fitting procedure have to be checked by applying some additional restrictions in the model analysis of the ITC and DSC data.

For the model analysis of ITC data, such restriction is obtained by combining the rts model of micellization with the critical micelle concentration (cmc), defined by Phillips,[55] into

$$\Delta G_M^\circ = (RT/n)\left\{\ln\left(\frac{n^2(2n-1)}{(n-2)}\right) + (n-1)\ln\left(\frac{n(2n-1)}{(n-1)(2n+2)}\mathrm{cmc}\right)\right\} \quad (10)$$

According to Philips,[55] the cmc is determined from the criterion $(d^3\Phi/dc_2^3)_{cmc} = 0$, expressed in terms of a property Φ that can be defined relative to the state S as $\Phi = Ac_M$, where A is a constant and c_M is the concentration of micelles. It can be seen from eq 5 that Φ corresponds to the cumulative heat effect, $\int_0^{c_2} \Delta H\, dc_2$, which means that the measured ΔH versus c_2 curve is proportional to the $(d\Phi/dc_2)$ vs c_2 curve. Therefore, cmc can be determined independently from experimental data as the concentration c_2 at which $(d^2\Delta H/dc_2^2)_{cmc} = 0$, and using this cmc value, ΔG_M° can be expressed at a given T only as a function of n (eq 10). Thus, in the analysis of ITC data, Philips's criterion can be used to check the influence of a high $n-\Delta G_M^\circ$ correlation on the best-fit values of the adjustable parameters by expressing ΔG_M° at a given T and cmc as a function of n. Furthermore, from the comparison of the best-fit values of n, ΔG_M°, and ΔH_M° obtained when all of them are adjustable parameters with those obtained using the ΔG_M° fixed by eq 10, one can determine whether the n, ΔG_M°, and ΔH_M° values obtained by the rts model are physically acceptable (see Supporting Information). At this point, we would like to emphasize that micellization can be treated also as a pseudo-phase separation (pps) process (a single-step process) occurring at the cmc. For this special case ($n = \infty$), it follows from eq 10 that $\Delta G_M^\circ = RT$ ln cmc, while ΔH_M° is simply the difference between the ΔH value above the cmc, where $(\partial(n_2\alpha_M)/\partial n_2)_{n_1,P,T} = 1$, and the ΔH value below the cmc, where $(\partial(n_2\alpha_M)/\partial n_2)_{n_1,P,T} = 0$ (see eq 5 and Figure 2a). Since the cmc can be estimated from Philips's criterion as described earlier, the ΔG_M°, ΔH_M°, and $T\Delta S_M^\circ$ ($= \Delta H_M^\circ - \Delta G_M^\circ$) values for the pps model at a given T are obtained from the experimental data without actual fitting the model function to the experimental ΔH vs c_2 curves. ΔH_M° values determined by rts and pps model analysis at different temperatures can be used to construct ΔH_M° versus T curves, from which the corresponding $\Delta C_{P,M}^\circ$ values (slopes) are obtained.

The physical meaning of the highly correlated n and $\Delta G_M^\circ(T_o)$ parameters obtained from the analysis of DSC data may be checked by the restriction derived from eqs 6 and 9 and the general condition that, at $T = T_{max}$ (peak of the DSC thermogram), the temperature derivatives of ΔC_P and α_M are $(\partial\Delta C_P/\partial T)_{n_1,n_2,P,T_{max}} = 0$ and $(\partial\alpha_M/\partial T)_{n_1,n_2,P,T_{max}} \neq 0$. This criterion, expressed as

$$3\Delta C_{P,M}^\circ - \frac{2\Delta H_M^\circ(T_{max})}{T_{max}} + \frac{\Delta H_M^\circ(T_{max})^2}{RT_{max}^{\,2}}\left[\frac{n(1-2\alpha_M)(1+(n-1)\alpha_M) - (n-1)n\alpha_M(1-\alpha_M)}{(1+(n-1)\alpha_M)^2}\right] = 0 \quad (11)$$

enables us to determine $\Delta G_M^\circ(T_o)$ from eqs 7 and 8 for a given set of n, $\Delta H_M^\circ(T_o)$, and $\Delta C_{P,M}^\circ$. Since the temperature of the maximum of the DSC thermogram, T_{max}, can be estimated directly from the experimental data, the model function (eq 6) may be fitted to the experimental thermograms using the adjustable parameters n, $\Delta H_M^\circ(T_o)$, and $\Delta C_{P,M}^\circ$. Similarly as with ITC, the difference in the best-fit values of the parameters n, $\Delta G_M^\circ(T_o)$, $\Delta H_M^\circ(T_o)$, and $\Delta C_{P,M}^\circ$ obtained when all of them are taken as adjustable parameters and those obtained with ΔG_M° fixed by eq 11 can be used as a measure of the physical meaning of these parameters (see Supporting Information).

Correlation between the Thermodynamic and Structural Parameters. Numerous studies on the transfer of model compounds from a pure organic phase into water and on protein folding have shown that, for the observed transitions, both $\Delta C_{P,trans}^\circ$ and ΔH_{trans}° can be parametrized in terms of the corresponding changes in the solvent-accessible nonpolar (ΔA_N) and polar (ΔA_P) surface areas of the solute molecules.[28,34−43] In this work, we used such parametrization to correlate $\Delta C_{P,M}^\circ$ and ΔH_M° with the ΔA_N and ΔA_P values that accompany

association of surfactant molecules into micelles. By modeling the micellization process as a transfer of surfactant molecules from aqueous solution into the micellar phase, one can express $\Delta C_{P,M}^\circ$ and ΔH_M° as sums of nonpolar (subscript N) and polar (subscript P) contributions:[27,30,44]

$$\Delta C_{P,M}^\circ = \Delta C_{P,N}^\circ + \Delta C_{P,P}^\circ = a\Delta A_N + b\Delta A_P \quad (12)$$

and

$$\Delta H_M^\circ = \Delta H_M^\circ(T_H) + \Delta C_{P,M}^\circ(T - T_H) = \Delta H_N^\circ + \Delta H_P^\circ$$
$$= [c + a(T - T_H)]\Delta A_N + [d + b(T - T_H)]\Delta A_P \quad (13)$$

The parameters $a = 1.9 \pm 0.1$ J mol^{-1} K^{-1} Å^{-2}, $b = -1.1 \pm 0.1$ J mol^{-1} K^{-1} Å^{-2}, $c = -21.5 \pm 10$ J mol^{-1} Å^{-2}, and $d = 205 \pm 20$ J mol^{-1} Å^{-2} are obtained from the solubility of the model cyclic dipeptides in water, while $T_H = 60$ °C is the selected reference temperature at which $\Delta H_M^\circ(T_H)$ is parametrized as $\Delta H_M^\circ(T_H) = c\Delta A_N + d\Delta A_P$.[44]

According to the described model of micellization, the corresponding entropy of micellization, ΔS_M°, can be expressed as[40−45]

$$\Delta S_M^\circ = \Delta S_{M,solv}^\circ + \Delta S_{M,other}^\circ \quad (14)$$

where $\Delta S_{M,solv}^\circ$ is the entropy change resulting from the changes in solvation of the surfactant molecules upon their transfer from aqueous solution into the micellar phase, and the part $\Delta S_{M,other}^\circ$ contains all other contributions to ΔS_M°. It has been shown that the entropy change accompanying the processes involving transfer of nonpolar groups (surface area) from solid, liquid, and gas phases as well as from the protein interior to water converges at temperature $T_S \approx 112$ °C to the value of zero.[30,134] Accordingly, $\Delta S_{M,solv}^\circ$ may be estimated as $\Delta S_{M,solv}^\circ = \Delta C_{P,M}^\circ \ln(T/T_S)$, which amounts to about 13R at 25 °C (Figure 8d). As shown recently,[135,136] the energetics of protein folding and association can be correlated with the corresponding structural features through ΔA_N and ΔA_P values calculated using the experimentally determined values of ΔC_P° and ΔH°. We used the same approach for micellization of C_8E_Y ($Y = 4, 5, 6$) and calculated the corresponding ΔA_N and ΔA_P from eqs 12 and 13 (Figure 8). Furthermore, for each surfactant, $\Delta S_{M,other}^\circ$ was estimated by subtracting the calculated $\Delta S_{M,solv}^\circ = \Delta C_{P,M}^\circ \ln(T/T_S)$ from the corresponding measured ΔS_M° (eq 14; Figure 8d).

The ΔA_N and ΔA_P values can also be estimated from the structural features of the studied micellization processes. Analysis of SAXS measurements performed on the surfactant solutions studied in this work shows that the micelles formed from C_8E_Y ($Y = 4, 5, 6$) surfactants can be considered as spherical particles, with the radius of the water-inaccessible nonpolar core about 1.3 nm (Figure 4). Moreover, it suggests that, in the micelles, the ether parts, E_Y, of the C_8E_Y molecules are largely exposed to water (Figure 4). Since the experimental SAXS observations are confirmed also by molecular dynamics simulation of C_8E_Y micelles in water,[108] one may assume that, upon transfer from the monomeric to the micellar form, only the C_8 part of the molecule is removed from the water and transferred to the nonpolar core. It follows that the corresponding ΔA_N may be estimated as $\Delta A_N = -A_N(C_8)$, where $A_N(C_8)$ is the water-accessible surface area of the C_8 part in aqueous solution. To obtain $A_N(C_8)$, the most populated conformations of C_8E_Y observed in the above-mentioned molecular dynamics simulation (dihedral angles: C−C−C−C predominantly trans, C−C−O−C mostly trans, and O−C−C−O mostly gauche(±)) were reconstructed by using the program package CS Chem3D Pro. $A_N(C_8)$ was calculated for every conformation using the method introduced by Tsodikov et al.[121] Finally, for each surfactant, $A_N(C_8)$ was computed as the conformational average: $A_N(C_8) = (\sum_i A_N(C_8)_i\, e^{-E_i/RT})/\sum_i e^{-E_i/RT}$, where $A_N(C_8)_i$ is the water-accessible surface area of the C_8 part of the ith C_8E_Y conformation, E_i is the corresponding energy calculated using the MM2 force field, and $T = 298.15$ K. The so-obtained average values are practically the same for C_8E_4, C_8E_5, and C_8E_6: $\Delta A_N = -A_N(C_8) = -225 \pm 15$ Å^2. By contrast, there is no evidence of significant changes of the polar accessible surface

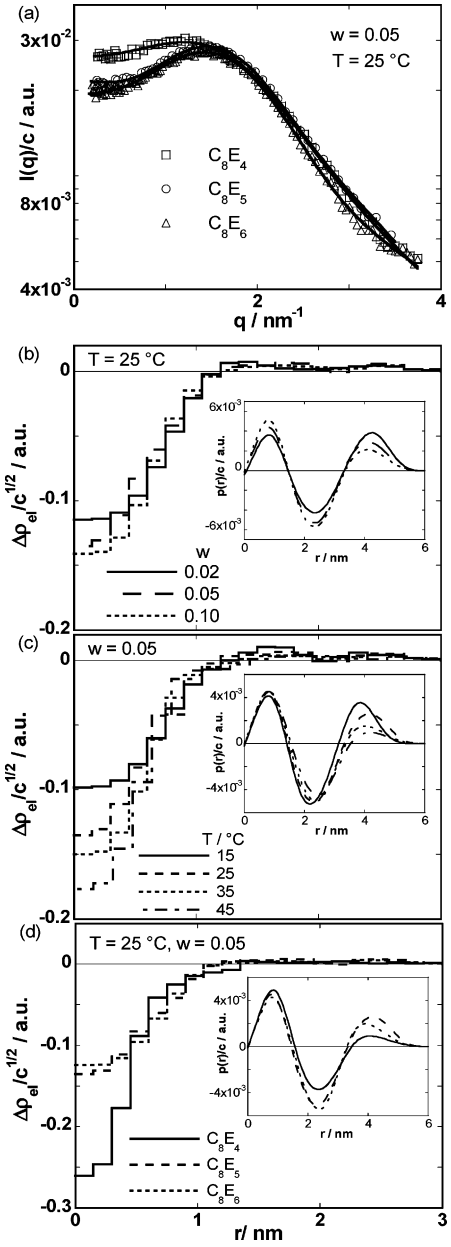

Figure 4. (a) Experimental SAXS spectra of C_8E_4, C_8E_5, and C_8E_6 aqueous solutions (symbols; w = weight fraction) as functions of scattering vector q and fits to the experimental data obtained by the indirect Fourier transformation (IFT) (lines). (b,c) Electron density contrast profiles, $\Delta\rho_{el}$, of C_8E_5 micelles in water, normalized by the square root of the surfactant concentration and the corresponding normalized pair−distance functions, $p(r)$. Insets: Variation of $p(r)/c$ with composition (panel b) and temperature (panel c). (d) Normalized electron density contrast profiles, $\Delta\rho_{el}$, of C_8E_4, C_8E_5, and C_8E_6 micelles in water and the corresponding normalized pair−distance distribution functions, $p(r)$ (inset). All profiles were calculated from the experimental scattering curves by IFT and square root deconvolution (DECON).

areas upon micellization for any of the three surfactants (Figure 4). Therefore, their ΔA_P values were estimated to be $\Delta A_P = 0 \pm 15$ Å^2. These structure-based estimates of the ΔA_N and ΔA_P values were then used to estimate the corresponding values of $\Delta C_{P,M}°$ (eq 12), $\Delta H_M°$ (eq 13), and $\Delta S_{M,solv}°$ (eq 14). Since C_8E_Y surfactants appear to form spherical micelles with the C_8 alkyl chains incorporated in their hydrophobic cores, the structure-based value of $n = 27 \pm 5$ can be estimated according to the approach described by Tanford.[80]

In an attempt to interpret and estimate $\Delta S_{M,other}°$ on the basis of changes in the architecture and behavior of the surfactant molecules that occur upon micellization, we discussed it as a sum of the corresponding translational, conformational, and size contributions. We divided the micellization process into three hypothetical steps,

$$\text{S(solution)} \xrightarrow{\Delta S_{SS}°} \text{S(pure phase)} \xrightarrow{\Delta S_{SM}°} (1/n)\text{M(pure phase)} \xrightarrow{\Delta S_{MM}°} (1/n)\text{M(solution)}$$

and since solvation changes accompanying the micellization are already taken into account by the $\Delta S_{M,solv}°$ term (eq 14), all surfactant molecules involved in the three transfer steps are considered to be unsolvated. Thus, $\Delta S_{M,other}°$ may be expressed as $\Delta S_{M,other}° = \Delta S_{SS}° + \Delta S_{SM}° + \Delta S_{MM}°$, where $\Delta S_{SS}°$ corresponds to the transfer of unsolvated surfactant molecules from the hypothetical 1 M aqueous solution into the pure liquid phase, $\Delta S_{SM}°$ is the contribution due to the ordering of surfactant monomers in the pure organic phase into their micellar form, and $\Delta S_{MM}°$ represents the contribution due to the transfer of micelles from the pure organic phase into the hypothetical 1 M aqueous solution of unsolvated micelles. The first hypothetical step can be discussed in terms of the Flory−Huggins (FH) lattice theory, and the resulting estimate takes into account the size of the solute and solvent molecules and the changes in translation and conformation of the polymer (surfactant) molecules.[137] For the second step, a rough estimate of $\Delta S_{SM}°$ can be made on the basis of a simple model of packing of alkyl-chain amphiphilic molecules into spherical micelles introduced by Gruen.[110−112] This model allows estimation of the conformational entropy change resulting from the transfer of alkyl chains from the random-coil state characteristic for *n*-alkane into the micelles. On incorporation into the micelles, the alkyl chains lose a significant number of gauche (±) bonds, and for C_8 chains the resulting conformational entropy change is estimated to be around $-1(\pm1)R$. Our estimate of $\Delta S_{MM}°$ that results from the transfer of spherical micelles from the organic phase into aqueous solution is based on the assumption that, upon transfer, the conformation of the micelles stays about the same. This means that $\Delta S_{MM}°$ will reflect only the changes in translational entropy and different sizes of solute and solvent molecules. Following the excellent discussion on theoretical treatment of transfer processes by Chan and Dill,[137] we estimated $\Delta S_{MM}°$ using the approach described by Sharp et al.[138] It is based on the approximation of liquid-state entropies by ideal-gas entropies and leads to an expression for $\Delta S_{MM}°$ that is similar to the corresponding FH expression, in which the terms reflecting the conformational entropy are neglected. By estimating the partial molar volumes of surfactant from the corresponding density measurements, one obtains that, for $n \gg 1$, the $\Delta S_{SS}°$ and $\Delta S_{MM}°$ contributions almost cancel out (see Supporting Information), which further means that $\Delta S_{M,other}° \approx \Delta S_{SM}°$. The importance of this estimation is not the value of $\Delta S_{M,other}°$ itself, but the fact that $\Delta S_{M,other}°$ is much smaller than $\Delta S_{M,solv}°$ (only about 10% of $\Delta S_{M,solv}°$).

The energetics of micellization ($\Delta C_{P,M}°$, $\Delta H_M°$, $\Delta S_M°$, $\Delta G_M°$, and n), based on information obtained from structural and theoretical analysis, is now completely defined and can be compared to the corresponding experimental thermodynamic observations.

Results

Isothermal Titration Calorimetry (ITC). Typical raw ITC and DSC signals resulting from demicellization−micellization of C_8E_Y, together with the SAXS signals, are presented in Figure 1. As shown by calorimetric demicellization titration curves constructed from the raw ITC data (Figure 2a,b), micellization of C_8E_Y may be considered as a pps process occurring at the cmc (Figure 2a). However, such a one-step process fails to describe the experimental points in the transition region. By contrast, the rts model of micellization (eqs 5, 7−10) describes very well the entire ITC titration curve and appears to be, therefore, much more realistic than the pps model. $\Delta H_M°$ values determined at different T by pps and rts model analysis show constant $d\Delta H_M°/dT$ slopes, indicating that the corresponding $\Delta C_{P,M}°$ values may be treated as temperature-independent quantities. Moreover, for all the surfactants studied, the n values determined by rts model analysis decrease slightly with increasing temperature; however, due to the simplicity of thermodynamic modeling, we assumed n to be a temperature-independent quantity. The effect of such an assumption on the shape of the best-fit model ITC titration curves (Figure 2) can be checked by performing a global fitting of the model function (eq 5) to the family of the ITC curves measured at various temperatures, using the adjustable parameters $\Delta G_M°(T_o)$, $\Delta H_M°(T_o)$, and $\Delta C_{P,M}°$ and a single value of n, and comparing it to the individual fittings (Figure 2b). As shown in Figure 2b−d, the assumption that $n \neq n(T)$ appears to be reasonable. Moreover, we observed good agreement between the thermodynamic parameters of C_8E_Y micellization obtained by the described ITC data analysis (Table 1) and the available thermodynamic data measured on similar systems.[73,139−143]

Differential Scanning Calorimetry (DSC). DSC thermograms of C_8E_Y measured in the 1−100 °C range show low- and high-temperature transitions. High-temperature transitions were observed before[140,141] and may be ascribed to a phase separation of C_8E_Y solutions. According to our DSC measurements, they occur at about 47 (C_8E_4), 66 (C_8E_5), and 68 °C (C_8E_6) (Supporting Information). On the other hand, repetitive scans below the phase separation temperature, performed at various surfactant concentrations, suggest that the observed low-temperature transition may be considered as a reversible micellization process (Figure 1c). This is confirmed by the fact that the temperature dependences of ΔC_P, ΔH, and ln Δ derived from the rts model (see eq 6 and the corresponding text) display very good agreement with the corresponding model-independent (experimental) quantities (Figure 3a). In addition to the assumption that n and $\Delta C_{P,M}°$ are temperature-independent quantities, the applied rts model analysis (eqs 6, 7−9, 11) assumes that the parameters n, ΔH_M, and $\Delta C_{P,M}$ do not depend on the surfactant concentration, c_2. To check the appropriateness of this assumption, simultaneous (global) fitting of the model function (eq 6) to the family of the DSC thermograms measured at different surfactant concentrations was performed (Figure 3b). The global fit agrees well with the corresponding best fits of the model function to each thermogram measured at different surfactant concentrations (Figure 3b). Since the agreement is reflected also in the corresponding temperature dependences of α_M and $(\partial\alpha_M/\partial T)_{n_1,n_2,P}$ (Figure 3c,d), the above assumptions seem

TABLE 1: Thermodynamic Parameters of C_8E_4, C_8E_5, and C_8E_6 Micellization in Aqueous Solutions at 25 °C, Obtained by Model Analysis of Calorimetric (ITC, DSC) Data[a] and by Structure-Based Calculations[b]

method	$\Delta G_M°$/ kJ mol^{-1}	$\Delta H_M°$/ kJ mol^{-1}	$T\Delta S_M°$/ kJ mol^{-1}	$\Delta C_{P,M}°$/ kJ mol^{-1}K^{-1}	cmc/ mmol L^{-1}	n
			C_8E_4			
ITC-pps	−11.5	15.7	27.2	−0.39	9.6	/
ITC-rts	−10.7	16.7	27.4	−0.40	9.3	30
DSC-rts	−10.8	15.2	26.0	−0.40	8.7	30
			C_8E_5			
ITC-pps	−11.5	17.2	28.7	−0.40	9.8	/
ITC-rts	−10.5	18.7	29.2	−0.42	9.6	28
DSC-rts	−10.5	17.9	28.4	−0.43	8.8	22
			C_8E_6			
ITC-pps	−11.7	18.5	30.1	−0.42	9.0	/
ITC-rts	−10.6	19.8	30.4	−0.45	8.7	25
DSC-rts	−10.6	18.0	28.6	−0.46	8.5	23
structure[b]	−10	20	30	−0.42	10	27

[a] The relative errors estimated from repetitive ITC measurements are ±0.01 ($\Delta G_M°$), ±0.02 ($\Delta H_M°$), ±0.01 ($T\Delta S_M°$), ±0.05 ($\Delta C_{P,M}°$), ±0.03 (cmc), and ±0.1 (n). The corresponding errors resulting from DSC measurements are about 2 times higher. pps = pseudo-phase separation model; rts = reversible two-state model. [b] The thermodynamic parameters obtained by structure-based calculation (eqs 12−14). Since the estimated changes in the solvent-accessible surface areas appear to be the same for all three surfactants, only a single set of structure-based parameters is presented. The relative errors that resulted from the appropriate propagation are ±0.5 ($\Delta G_M°$), ±0.2 ($\Delta H_M°$), ±0.1 ($T\Delta S_M°$), ±0.1 ($\Delta C_{P,M}°$), ±2 (cmc), and ±0.2 (n). The value of n was estimated according to the approach of Tanford.[80]

to be justified. Moreover, the thermodynamic parameters of C_8E_Y micellization obtained by rts analysis of DSC data agree well with those obtained by the corresponding analysis of ITC data (Table 1, Figure 7). Thus, ITC and DSC data analysis strongly suggest that the rts model, assuming $n \neq n(T,c_2)$, $\Delta H_M = \Delta H_M° \neq \Delta H_M(c_2)$, and $\Delta C_{P,M} = \Delta C_{P,M}° \neq \Delta C_{P,M}(T,c_2)$, is an appropriate model for description of the concentration and temperature dependence of the studied micellization processes in the measured temperature and concentration intervals.

Small-Angle X-ray Scattering (SAXS). As shown in Figure 1d, the general shape of the scattering curves for C_8E_Y micellar aqueous solutions remains unaltered for all compositions at constant temperature. However, at small angles, we observe a slight increase of scattering with increasing temperature (Figure 1e). A special feature of these curves is a pronounced downturn of the scattering intensity at low values of the scattering vector. This is a typical behavior of samples with a low overall contrast in the electron density.[88] SAXS spectra were evaluated utilizing the indirect Fourier transform method (ITF),[124,125] without taking into account interparticle interference. It has been shown for C_8E_4 aqueous solutions[88] that, at low surfactant concentrations (weight fraction <10%), such an approximation is reasonable. The same behavior has been observed for all systems investigated in this work.

As shown in Figure 4b,c the qualitative shape of the pair−distance distribution functions, $p(r)$, i.e., the shape of the C_8E_Y particles formed in the solution, does not change significantly upon varying the solution composition or temperature. Inspection of Figure 4b−d also shows that the shapes of the C_8E_Y $p(r)$ functions are characteristic for the heterogeneous spherical micelles with the difference in the core and the shell scattering contrast.[144,145] Typical distributions of the electron density contrast within the C_8E_Y micelles, resulting from the deconvolution of the corresponding $p(r)$ function[126−129] presented in Figure 4b−d, show two regions of opposite sign. By taking into account the molar volumes of alkyl and oxyethylene chains,[146,147] the electron density of the nonpolar part (C_8) can be estimated to be about 297 e$^-$ nm^{-3}. The corresponding electron densities of the ether parts (E_Y) are 405, 400, and 398 e$^-$ nm^{-3} for C_8E_4, C_8E_5, and C_8E_6, respectively. The electron density of pure water is 334 e$^-$ nm^{-3}, which means that the C_8 hydrophobic cores have negative and the E_Y shells positive scattering contrasts against the water. Furthermore, these estimations suggest higher values of the positive scattering contrast than those observed experimentally (Figure 4b−d). Since the hydrated water may substantially decrease the average electron density of the E_Y shells, the observed deviations may be ascribed to a strong hydration of the E_Y parts of the micelles. The same behavior has been observed for C_8E_4 [88] and Brij35[145] in aqueous solution.

The radius of the hydrophobic core can be estimated as the r value at which the scattering contrast changes sign (Figure 4b−d). In Figure 4d is presented a comparison of the excess electron density profiles for C_8E_4, C_8E_5, and C_8E_6 at 25 °C. Estimates of the C_8E_Y micelle hard-core radii were obtained

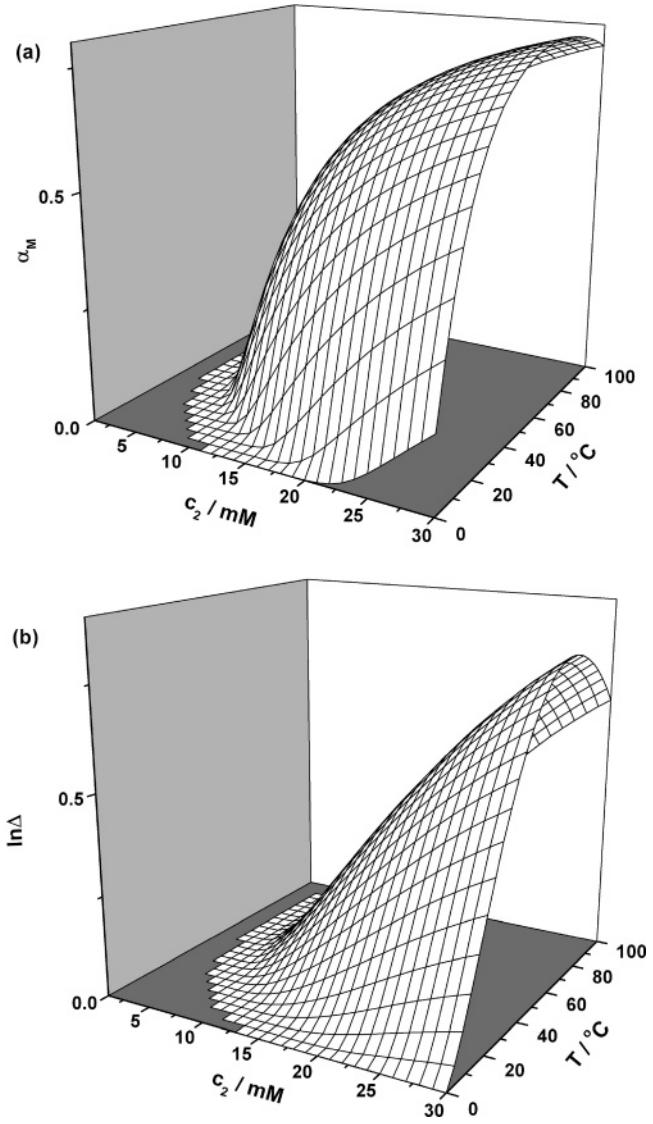

Figure 5. Fraction of C_8E_6 molecules in the micellar form, α_M (panel a), and the corresponding logarithm of the relative partition function, ln Δ (panel b; see eq 6), as functions of total surfactant concentration, c_2, and temperature, T, obtained from the reversible two-state model (rts; eq 8) analysis of ITC data (Table 1), assuming the validity of the rts model in the calculated temperature interval.

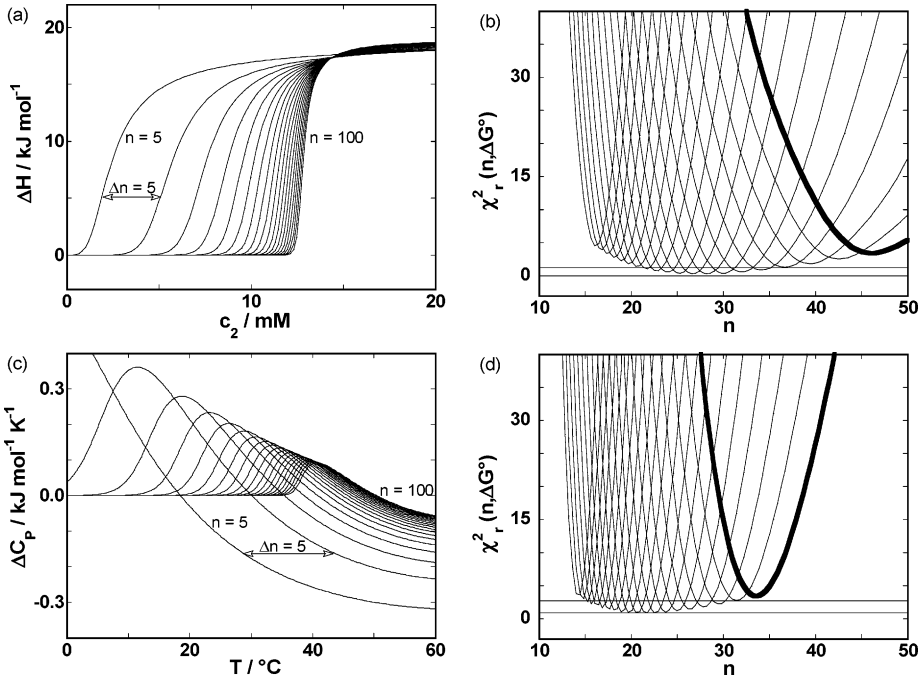

Figure 6. Simulations of ITC (panel a; for $\Delta G_M^\circ = -10.5$ kJ mol^{-1} and $\Delta H_M^\circ = 19.0$ kJ mol^{-1} at 25 °C; see eq 5) and DSC (panel c; for $\Delta G_M^\circ(T_o) = -10.4$ kJ mol^{-1}, $\Delta H_M^\circ(T_o) = 17.9$ kJ mol^{-1}, $T_o = 25$ °C, and $\Delta C_{P,M}^\circ = -0.43$ kJ mol^{-1} K^{-1} at $c_2 = 9.92$ mM; see eq 6) curves for various values of aggregation numbers (n) based on the reversible two-state model (rts; eq 8). Thermodynamic parameters used for the simulations are taken from the best rts fits of ITC and DSC data presented in Figures 2a and 3a, respectively. For the same data sets, the chi-square function, reduced to the number of degrees of freedom, χ^2_r (see Supporting Information), as a function of n and $\Delta G_M^\circ(T_o)$ (varying from -10.85 (bold line) to -9.90 kJ mol^{-1} in steps of 0.05 kJ mol^{-1}), is presented in panels b (ITC) and d (DSC). If one treats both n and $\Delta G_M^\circ(T_o)$ as adjustable parameters, all their values that fall into the shaded area between the two horizontal lines would fit the experimental data equally well. The size of this area is obtained by fitting the model function to the experimental ITC and DSC data presented in Figures 2a and 3a for various c_2 in the $c_2(1 \pm 0.02)$ interval and various estimated baseline adjustments describing $\bar{H}_S$ (ITC) and $\bar{C}_{P,S}$ (DSC).

from the intersect of these profiles with the abscissa at $r \approx 1.4$ nm (C_8E_4) and $r \approx 1.2$ nm (C_8E_5, C_8E_6). An example of the variation of the excess electron density profile with temperature is shown in Figure 4c. Since the input pair−distance distribution functions do not differ significantly, the resulting excess electron density profiles have the same shape at all measured temperatures. In principle, the maximal particle (micelle) dimensions can be determined as the vanishing point of the corresponding contrasts in the electronic density. In our case, however, these points, and therefore the largest particle dimensions, cannot be read distinctively from $\Delta\rho_{el}/c^{1/2}$ vs r graphs, because for each surfactant the contrast in the electron density beyond the nonpolar core radius is too low (Figure 4b−d; see Supporting Information).

Discussion

Limitations of Quantitative Analysis of ITC and DSC Signals Accompanying the Micellization or Demicellization Process. The necessary conditions to observe the ITC or DSC signal resulting from micellization−demicellization are $\Delta H_M^\circ(T) \neq 0$ and $(\partial(n_2\alpha_M)/\partial n_2)_{n_1,P,T} \neq 0$ (ITC) or $\Delta H_M^\circ(T) \neq 0$ and $(\partial\alpha_M/\partial T)_{n_1,n_2,P} \neq 0$ (DSC). Thus, when $\Delta H_M^\circ(T) \neq 0$, a successful performance of ITC or DSC experiments requires a proper selection of surfactant concentration and temperature range in which significant changes in the micellization partition function can occur (Figure 5). In other words, ITC and DSC signals reflect changes of population of any thermodynamic (macro) state accessible to the surfactant molecules (Figure 5). The simplest way to define the best working conditions for ITC or DSC experiment is to simulate the signals on the basis of a thermodynamic model (Figures 5 and 6a,c), which requires thermodynamic data that can be estimated, as shown in this work, from the micellar structural features.

The simplest model capable of adequately describing ITC and DSC signals accompanying a micellization−demicellization process is a reversible two-state model (eqs 5−9, Figures 2 and 3). For its fitting to the experimental data, three (ITC: n, ΔG_M°, ΔH_M°) or four (DSC: n, $\Delta G_M^\circ(T_o)$, $\Delta H_M^\circ(T_o)$, $\Delta C_{P,M}^\circ$) parameters are needed. With this setup of parameters, we achieved a very good fit of the rts model to the experimental ITC curves and DSC thermograms (Figures 2 and 3). The question that always arises with such fittings is whether there exists a high reciprocal correlation between some pairs of adjustable parameters (see Supporting Information). Indeed, for the three surfactants, almost total correlation (± 1) between the parameters n and ΔG_M° was observed in the analysis of ITC and DSC micellization data, meaning that different pairs of n and ΔG_M° may give equally good fits to the corresponding experimental curves. This can be clearly seen from the shape of χ^2 as a function of n and ΔG_M°, which forms a valley that results from the fact that practically the same ITC and DSC curves can be constructed for various combinations of n and ΔG_M° (Figure 6a,c). Consequently, the true errors in n and ΔG_M° may be significantly higher than those obtained by taking square roots of the diagonal elements of the variance−covariance matrix constructed from a single fit of the data set. Since, in the published studies dealing with the analysis of ITC and DSC micellization−demicellization signals, practically no attention has been paid to this problem, we would like to show that high correlation between adjustable parameters may be avoided to a certain extent (see Supporting Information) by expressing ΔG_M° as a function of n at a given cmc (ITC; eq

10) and as a function of n, $\Delta H_M°$, and $\Delta C_{P,M}°$ at a given T_{max} (DSC; eq 11). In other words, the conditions given by eqs 10 and 11 can be used to check the physical meaning of the adjustable parameters n and $\Delta G_M°$. Whenever the fit was statistically good and the cmc (ITC) or T_{max} (DSC) determined from the best-fit model function agreed with the corresponding experimentally determined values within the error of Δcmc $= \pm 0.3$ mM and $\Delta T_{max} = \pm 0.5$ K, we considered the obtained n and $\Delta G_M°$ values as physically acceptable quantities.

We have shown that both ITC and DSC can be successfully used as independent methods for determination of thermodynamic parameters of micellization, including the aggregation number. By using DSC we benefit, since estimates of n, $\Delta G_M°$, $\Delta H_M°$, and $\Delta C_{P,M}°$ can be obtained within a single DSC experiment.

Energetics of Micellization in Correlation with Structural Features. The thermodynamic analysis of the C_8E_Y micellization (Table 1) shows that, at 25 °C, $\Delta H_M°$ makes an unfavorable and $T\Delta S_M°$ a highly favorable contribution to $\Delta G_M°$. This effect is more pronounced with the elongation of the ether part of the surfactant molecule. The enthalpy−entropy compensation results in about the same $\Delta G_M°$ values for C_8E_4, C_8E_5, and C_8E_6. At concentrations around the cmc, micelles contain from about 30 (C_8E_4) to about 25 (C_8E_5, C_8E_6) monomers. $\Delta C_{P,M}°$ is slightly less negative for C_8E_4 than for C_8E_5 and C_8E_6. The observed differences in $\Delta H_M°$, $T\Delta S_M°$, and $\Delta C_{P,M}°$ between C_8E_4 (hydrophobic core radius $r \approx 1.4$ nm) and C_8E_5, C_8E_6 ($r \approx 1.2$ nm) may be ascribed to a slightly higher fraction of buried nonpolar surface area upon micellization of C_8E_5 and C_8E_6 (Figure 8a).

The temperature dependences $\Delta G_M°$, $\Delta H_M°$, $T\Delta S_M°$, cmc, and ln Δ obtained from ITC and DSC by various types of model analysis are in good agreement with the corresponding parameters estimated from structure-based calculations (Figure 7, Table 1). Inspection of Table 1 shows that the aggregation numbers agree well with the corresponding values estimated according to Tanford[80] using the results of SAXS measurements that show complete burial of the C_8 parts of C_8E_4, C_8E_5, and C_8E_6 molecules within the spherical micelle cores (Figure 4). It can be seen from Figure 8a,b that experimental thermodynamic-based and structure-based estimates of changes in accessible surface areas and $\Delta C_{P,M}°$ (eqs 12 and 13) are determined merely by removal of the nonpolar surface from water upon micellization. The dissection of $\Delta H_M°$ at 25 °C (eq 13) shows that the enthalpy change due to the interactions of nonpolar surfaces is highly unfavorable, while the corresponding contribution due to the interactions of polar surfaces can be neglected (Figure 8c). Similarly, the dissection of $T\Delta S_M°$ (eq 14; Figure 8d) shows that the main driving force of micellization is the $T\Delta S_{M,solv}°$ contribution, which results from much higher hydration of surfactant molecules in their free monomeric form and can be expressed as $T\Delta S_{M,solv}° = T\Delta C_{P,M}° \ln(T/T_S)$.[30,134] Based on this estimation is the evaluation of the $T\Delta S_{M,other}°$ contribution, $T\Delta S_{M,other}° = T\Delta S_M° - T\Delta S_{M,solv}°$, which may be considered as an independent experimental approximation of the entropy contribution due to the loss of conformational, translational, and rotational freedom upon micellization (Figure 8d). Such experimental approximations of $T\Delta S_{M,other}°$, as well as the corresponding theoretical estimates discussed earlier, appear to be much less unfavorable than the entropy contribution due to the loss of translational and rotational degrees of freedom that would result from a rigid-body association ($T\Delta S_{r+t}° = -62.4$ kJ mol^{-1} at 25 °C).[37,148,149] This suggests that self-assembling of C_8E_4, C_8E_5, and C_8E_6 molecules into micelles is far from a rigid-body association, indicating the dynamic nature of micellar aggregates.

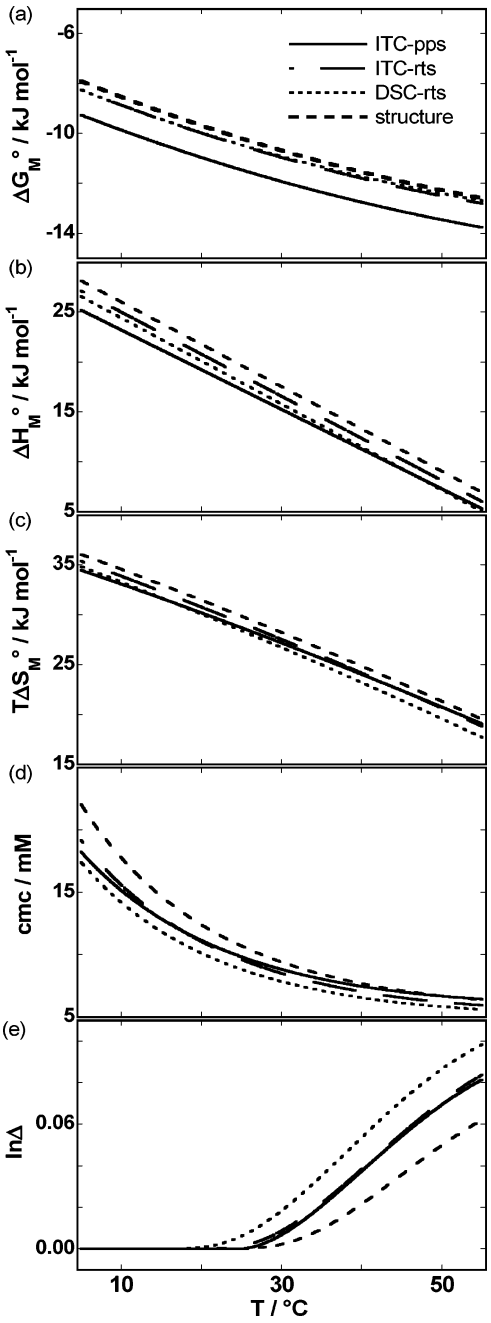

Figure 7. Comparison of thermodynamic parameters of C_8E_5 micellization as functions of temperature, obtained by various methods (pps = pseudo-phase separation model, rts = reversible two-state model, structure = structure-based calculation). Standard Gibbs free energy (panel a) and enthalpy of micellization (panel b), the corresponding entropy contribution (panel c), critical micelle concentration determined using a Philips's criterion (eq 10 for a given $\Delta G_M°$ and n; panel d), and relative partition function (see eq 6 and the corresponding text; $c_2 = 9.92$ mM; panel e).

We have shown that the structure-based parametrization of some basic thermodynamic quantities derived from the transfer of model compounds from a pure organic phase into water[26,27,30,44] can be used to predict reasonably well (Table 1, Figures 7 and 8) the energetics of micellization processes (parametrizations based on protein unfolding energetics data[44] also lead to a reasonably good agreement with the experiment). Unfortunately, it misses small but detectable differences in the

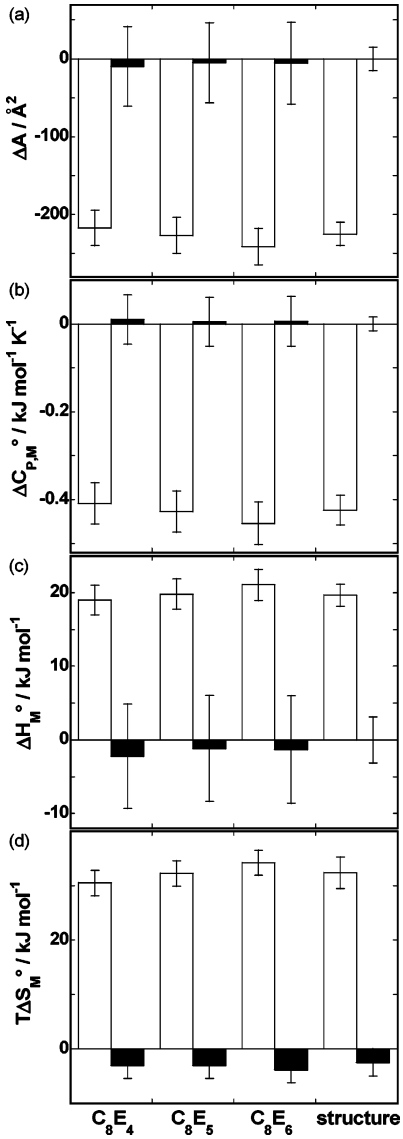

Figure 8. Dissection of experimental energetics of C_8E_4, C_8E_5, and C_8E_6 micelle formation at 25 °C in comparison to the corresponding structure-based calculation (eqs 12−14). (a) Changes in nonpolar (white columns; ΔA_N) and polar (black columns; ΔA_P) solvent-accessible surface areas upon micellization. (b) Contributions to the standard heat capacity of micellization due to the burial of nonpolar (white columns; $\Delta C_{P,N}°$) and polar (black columns; $\Delta C_{P,P}°$) surfaces (eq 12). (c) Contributions to the standard enthalpy of micellization due to the changed interactions of nonpolar (white columns; $\Delta H_N°$) and polar (black columns; $\Delta H_P°$) surfaces (eq 13). (d) The corresponding entropy contributions (eq 14) due to the differences in solvation of the surfactant monomer in the micellar form and in free form (white columns; $T\Delta S_{M,solv}°$) and other contributions that contain the loss of conformational, translational, and rotational freedom (black columns; $T\Delta S_{M,other}°$)

measured energetics of C_8E_4, C_8E_5, and C_8E_6 micellization (Table 1), most likely due to the errors in the parametrization itself and in the structural modeling based on SAXS measurements. Thus, to improve our understanding at the molecular level of processes such as micellization or some more complex binding or folding events that involve charged particles (see, for example, problems in interpreting the thermodynamics of drug−DNA association[150−154]), better models of solvation are needed. A promising step in this direction is modeling studies of water in the presence of nonpolar solutes, showing that the mechanism of hydrophobic solvation depends on the size and shape of the solute.[11,155] These studies suggest that inserting the small, nonpolar solute at room temperature into water creates a cage-like ordering ($\Delta S° < 0$) in which the first-shell water molecules have better hydrogen bonds, on average ($\Delta H° < 0$).[11,155] It seems that micellization of C_8E_Y surfactants in aqueous solution at 25 °C is governed by the same molecular driving forces, since removing the alkyl chains from water (dehydration of CH_2 and CH_3 groups) is accompanied by $\Delta H_M° > 0$ and $\Delta S_M° > 0$.

It is by no means a straightforward accomplishment to relate structural parameters of micelles and energetics of micellization. We have shown that this can be done using experimental thermodynamic and structural information in combination with the appropriate theoretical estimates. Several excellent publications have appeared recently, indicating that the additivity approach, including parsing of thermodynamics to nonpolar and polar contributions, can be successfully applied for describing the energetics of various interacting systems.[30,36−45,150,152−154] This approach is relatively simple; however, it has a shortcoming of involving at least one unmeasurable component (in our case, $\Delta S_{M,other}°$) that must be derived by means of some theoretical model. Moreover, entropy contributions are often not additive.[156] It has been shown by statistical mechanics that, in pure organic phases (micelle nonpolar core), translations are coupled to the polymer conformations.[137] Therefore, the entropy of micellization may involve terms of this type. In the case of C_8E_Y micellization, the agreement between $\Delta S_{M,other}°$ determined from the experimental thermodynamic cycle (eq 14, Figure 8d) and the corresponding theoretical estimate (see Thermodynamic Analysis) suggests that coupling of surfactant molecule translation to its conformation in the micellar form may be successfully treated by the Flory−Huggins theory.

Acknowledgment. This work was supported by the Ministry of Higher Education, Science and Technology and by the Agency for Research of Republic of Slovenia through Grants Nos. P1-0201 and J1-6653. M.B.-R. would like to express her gratitude to the Alexander von Humboldt Foundation, Germany, for the donation of the small X-ray scattering system.

Supporting Information Available: Details on the model analysis of ITC and DSC signals and on estimation of contributions to micellization entropy other than solvation, DSC thermograms showing low- (micellization) and high- (phase separation) temperature transitions, and information on the analysis of SAXS data regarding the estimation of maximal micelle dimension. This material is available free of charge via the Internet at http://pubs.acs.org.

References and Notes

(1) Tanford, C. The *Hydrophobic Effect: Formation of Micelles and Biological Membranes*, 2nd ed.; Wiley: New York, 1980.
(2) Stillinger, F. H. *Science* **1980**, *209*, 451.
(3) Ben-Naim, A. *Hydrophobic Interactions*; Plenum Press: New York, 1980.
(4) Dill, K. A. *Biochemistry* **1990**, *29*, 7133.
(5) Blokzijl, W.; Engberts, J. B. F. N. *Angew. Chem., Int. Ed. Engl.* **1993**, *32*, 1545.
(6) Oas, T. G.; Toone, E. J. *Adv. Biophys. Chem.* **1997**, *6*, 1.
(7) Scheraga, H. A. *J. Biomol. Struct. Dyn.* **1998**, *16*, 447.
(8) Hummer, G.; Garde, S.; Paulaitis, M. E.; Pratt, L. R. *J. Phys. Chem. B* **1998**, *102*, 10469.
(9) Southall, N. T.; Dill, K. A.; Haymet, A. D. J. *J. Phys. Chem. B* **2002**, *106*, 521.
(10) Chan, H. S.; Dill, K. A. *Annu. Rev. Biomol. Struct.* **1997**, *26*, 425.
(11) Dill, K. A.; Bromberg, S. *Molecular driving forces: Statistical thermodynamics in chemistry and biology*; Garland Science (Taylor & Francis Group): New York, 2002.
(12) Dill, K. A. *Science* **1990**, *250*, 297.
(13) Gill, S. J.; Wadsö, I. *Proc. Natl. Acad. Sci.* **1976**, *73*, 2955.
(14) Honig, B.; Yang, A.-S. *Adv. Protein Chem.* **1995**, *46*, 27.

(15) Privalov, P. L. *Adv. Protein Chem.* **1979**, *33*, 167.
(16) Privalov, P. L.; Gill, S. J. *Adv. Protein Chem.* **1988**, *39*, 191.
(17) Vogl, T.; Hinz, H.-J.; Hedwig, G. R. *Biophys. Chem.* **1995**, *54*, 261.
(18) Wimley, W. C.; Creamer, T. P.; White, S. H. *Biochemistry* **1996**, *35*, 109.
(19) Wolfenden, R.; Radzicka, A. *Science* **1994**, *265*, 936.
(20) Yang, A.-S.; Sharp, K. A.; Honig, B. *J. Mol. Biol.* **1992**, *227*, 889.
(21) Brandts, J. F. *J. Am. Chem. Soc.* **1964**, *86*, 4302.
(22) Fauchére, J.-L.; Pliška, V. *Eur. J. Med. Chem.—Chim. Ther*. **1983**, *18*, 369.
(23) Kauzmann, W. *Adv. Protein Chem.* **1959**, *14*, 1.
(24) Liu, Y.; Bolen, D. W. *Biochemistry* **1995**, *34*, 12884.
(25) Nozaki, Y.; Tanford, C. *J. Biol. Chem.* **1971**, *246*, 2211.
(26) Murphy, K. P.; Gill, S. J. *Thermochim. Acta* **1990**, *175*, 11.
(27) Habermann, S. M.; Murphy, K. P. *Protein Sci.* **1996**, *5*, 1229.
(28) Nichols, N.; Sköld, R.; Spink, C.; Wadsö, I. *J. Chem. Thermodyn.* **1976**, *8*, 1081.
(29) Cabani, S.; Gianni, P.; Mollica, V.; Lepori, L. J. *Solution Chem.* **1981**, *10*, 563.
(30) Murphy, K. P.; Freire, E. *Adv. Protein Chem.* **1992**, *43*, 313.
(31) Eisenberg, D.; McLachlan, A. D. *Nature (London)* **1986**, *319*, 199.
(32) Hermann, R. B. *J. Phys. Chem.* **1972**, *76*, 2754.
(33) Lee, B.; Richards, F. M. *J. Mol. Biol.* **1971**, *55*, 379.
(34) Reynolds, J. A.; Gilbert, D. B.; Tanfort, C. *Proc. Natl. Acad. Sci. U.S.A.* **1974**, *71*, 2925.
(35) Rose, G. D.; Geselowitz, A. R.; Lesser, G. J.; Lee, R. H.; Zehfus, M. H. *Science* **1985**, *229*, 834.
(36) Makhatadze, G. I.; Privalov, P. L. *Adv. Protein Chem.* **1995**, *47*, 307.
(37) Spolar, R. S.; Record, M. T., Jr. *Science* **1994**, *263*, 777.
(38) Myers, J. K.; Pace, N. C.; Scholtz, M. *J. Protein Sci.* **1995**, *4*, 2138.
(39) Xie, D.; Freire, E. *Proteins: Struct., Funct. Genet.* **1994**, *19*, 291.
(40) Baker, B. M.; Murphy, K. P. *J. Mol. Biol.* **1997**, *268*, 557.
(41) Murphy, K. P.; Xie, D.; Thompson, K. S.; Amzel, L. M.; Freire, E. *Proteins: Struct., Funct. Genet.* **1994**, *18*, 63.
(42) Lee, K. H.; Xie, D.; Freire, E.; Amzel, L. M. *Proteins: Struct., Funct. Genet.* **1994**, *20*, 68.
(43) Freire, E. *Pure Appl. Chem.* **1997**, *69*, 2253.
(44) Robertson, A. D.; Murphy, K. P. *Chem. Rev.* **1997**, *97*, 1251.
(45) Spolar, R. S.; Ha, J.-H.; Record, M. T. *Proc. Natl. Acad. Sci. U.S.A.* **1989**, *86*, 8385.
(46) National Academy of Science Panel Report on Biomolecular Self-assembling Materials, 1996 (available from http://www.nap.edu/books/0309056284/html/5.html).
(47) Russel, W. B.; Saville, D. A.; Schowalter, W. R. *Colloidal Dispersions*; Cambridge University Press: Cambridge, UK, 1989.
(48) Hunter, R. J. *Introduction to Modern Colloid Science*; Oxford University Press: Oxford, UK, 1993.
(49) Fleming, K. G. *Curr. Opin. Biotechnol.* **2000**, *11*, 67.
(50) Fleming, K. G. *Methods Enzymol.* **2000**, *323*, 63.
(51) Maire, M.; Champeil, P.; Møller, J. V. *Biochim. Biophys. Acta* **2000**, *1508*, 86.
(52) Moroi, Y. *Micelles: Theoretical and Applied Aspects*; Plenum Press: New York, 1992.
(53) Holmberg, K.; Jönsson, B.; Kronberg, B.; Lindman, B. *Surfactants and Polymers in Aqueous Solution*, 2nd ed.; John Wiley & Sons Ltd.: Chichester, UK, 2003.
(54) van Os, N. M.; Haak, J. R.; Rupert, L. A. M. *Physico-Chemical Properties of Selected Anionic, Cationic, and Nonionic Surfactants*; Elsevier: Amsterdam, 1993.
(55) Philips, J. N. *Trans. Faraday Soc.* **1955**, *51*, 561.
(56) Goddart, E. D.; Hoeve, C. A. J.; Benson, G. C. *J. Phys. Chem.* **1957**, *61*, 593.
(57) Benjamin, L. *J. Phys. Chem.* **1964**, *68*, 3575.
(58) Corkill, J. M.; Goodman, J. F.; Tate, J. R. *Trans. Faraday Soc.* **1964**, *60*, 996.
(59) Woolley, E. M.; Burchfield, T. E. *J. Phys. Chem.* **1984**, *88*, 2155.
(60) Desnoyers, J. E.; Caron, G.; De Lisi, R.; Roberts, D.; Roux, A.; Perron, G. *J. Phys. Chem.* **1983**, *87*, 1397.
(61) Archer, D. G. *J. Solution Chem.* **1987**, *16*, 347.
(62) Blandamer, M. J.; Cullis, P. M.; Soldi, L. G.; Engberts, J. B. F. N.; Kacperska, A.; van Os, N. M.; Subha, M. C. S. *Adv. Colloid Interface Sci.* **1995**, *58*, 171.
(63) Paula S.; Süs, W.; Tuchtenhagen, J.; Blume, A. *J. Phys. Chem.* **1995**, *99*, 11742.
(64) Sarmiento, F.; del Rio, J. M.; Prieto, G.; Attwood, D.; Jones, M. N.; Mosquera, V. *J. Phys. Chem.* **1995**, *99*, 17628.
(65) Bijma, K.; Blandamer, M. J.; Engberts, J. B. *Langmuir* **1998**, *14*, 79.
(66) Blandamer, M. J.; Cullis, P. M.; Engberts, J. B. F. N. *J. Chem. Soc., Faraday Trans.* **1998**, *94*, 2261.
(67) De Lisi, R.; Fiscario, E.; Milioto, S. *J. Solution Chem.* **1988**, *17*, 1015.
(68) Inglese, A.; De Lisi, R.; Milioto, S. *J. Phys. Chem.* **1996**, *100*, 2260.
(69) Stodghill, S. P.; Smith, A. E.; O'Haver, J. H. *Langmuir* **2004**, *20*, 11387.
(70) Shimizu, S.; Pires, P. A. R.; El Seoud, O. A. *Langmuir* **2004**, *20*, 9551.
(71) Chatterjee, A.; Maiti, S.; Sanyal, S. K. *Langmuir* **2002**, *18*, 2998.
(72) Chatterjee, A.; Moulik, S. P.; Sanyal, S. K. *J. Phys. Chem. B* **2001**, *105*, 12823.
(73) Ohta, A.; Miyagishi, S.; Aratono, M. *J. Phys. Chem. B* **2001**, *105*, 2826.
(74) Majhi, P. R.; Blume, A. *Langmuir* **2001**, *17*, 3844.
(75) Heerklotz, H.; Seelig, J. *Biochim. Biophys. Acta* **2000**, *1508*, 69.
(76) Heerklotz, H.; Espand, R. M. *Biophys. J.* **2001**, *80*, 271.
(77) Beyer, K.; Leine, D.; Blume, A. *Colloids Surf. B: Biointerfaces* **2006**, *49*, 31.
(78) Hildebrand, A.; Garidel, P.; Neubert, R.; Blume, A. *Langmuir* **2004**, *20*, 320.
(79) Schick, M. J.; Atlas, S. M.; Eirich, F. R. *J. Phys. Chem.* **1962**, *66*, 1326.
(80) Tanford, C. *J. Phys. Chem.* **1972**, *76*, 3020.
(81) Podo, F.; Ray, A.; Nemethy, G. *J. Am. Chem. Soc.* **1973**, *95*, 6164.
(82) Dill, K. A.; Koppel, D. E.; Cantor, R. S.; Dill, J. D.; Bendedouch, D.; Chen, S.-H. *Nature (London)* **1984**, *309*, 42.
(83) Cabane, B.; Zemb, T. *Nature (London)* **1985**, *314*, 385.
(84) Barreiro-Iglesias, R.; Alvarez-Lorenzo, C.; Concheiro, A. *J. Therm. Anal. Calorim.* **2002**, *68*, 479.
(85) Li, Y.; Xu, R.; Bloor, D. M.; Penfold, J.; Holzwarth, J. F.; Wyn-Jones, E. *Langmuir* **2000**, *16*, 8677.
(86) Hayter, J. B.; Zulauf, M. *Colloid Polym. Sci.* **1982**, *260*, 1023.
(87) Glatter, O.; Fritz, G.; Lindner, H.; Brunner-Popela, J.; Mittelback, R.; Strey, R.; Egelhaaf, S. *Langmuir* **2000**, *16*, 8692.
(88) Lang, P.; Glatter, O. *Langmuir* **1996**, *12*, 1193.
(89) Haan, S. W.; Pratt, L. R. *Chem. Phys. Lett.* **1981**, *79*, 436.
(90) Wijmans, C. M.; Linse, P. *J. Phys. Chem.* **1996**, *100*, 12583.
(91) Floriano, M. A.; Caponetti, E.; Panagiotopoulos, A. Z. *Langmuir* **1999**, *15*, 3143.
(92) Guerin, C. B. E.; Szleifer, I. *Langmuir* **1999**, *15*, 7901.
(93) Milchev, A.; Bhattacharya, A.; Binder, K. *Macromolecules* **2001**, *34*, 1881.
(94) Groot, R. D. *Langmuir* **2000**, *16*, 7493.
(95) von Gottberg, F. K.; Smith, K. A.; Hatton, T. A. *J. Chem. Phys.* **1997**, *106*, 9850.
(96) Salaniwal, S.; Cui, S. T.; Cochran, H. D.; Cummings, P. T. *Langmuir* **2001**, *17*, 1773.
(97) Tieleman, D. P.; van der Spoel, D.; Berendsen, H. J. C. *J. Phys. Chem. B* **2000**, *104*, 6380.
(98) Marrink, S. J.; Tieleman, D. P.; Mark, A. E. *J. Phys. Chem. B* **2000**, *104*, 12165.
(99) Allen, R.; Bandyopadhyay, S.; Klein, M. L. *Langmuir* **2000**, *16*, 10547.
(100) Salaniwal, S.; Cui, S. T.; Cochran, H. D.; Cummings, P. T. *Ind. Eng. Chem. Res.* **2000**, *39*, 4543.
(101) Faeder, J.; Ladanyi, B. M. *J. Phys. Chem. B* **2000**, *104*, 1033.
(102) Bogusz, S.; Venable, R. M.; Pastor, R. W. *J. Phys. Chem. B* **2000**, *104*, 5462.
(103) Maillet, J. B.; Lachet, V.; Coveney, P. V. *Phys. Chem. Chem. Phys.* **1999**, *1*, 5277.
(104) Wymore, T.; Gao, X. F.; Wong, T. C. *J. Mol. Struct.* **1999**, *485*, 195.
(105) Bocker, J.; Brickmann, J.; Bopp, P. *J. Phys. Chem.* **1994**, *98*, 712.
(106) Shelley, J. C.; Sprik, M.; Klein, M. L. *Langmuir* **1993**, *9*, 916.
(107) Smit, B.; Hilbers, P. A. J.; Esselink, K.; Rupert, L. A. M.; Vanos, N. M.; Schlijper, A. G. *J. Phys. Chem.* **1991**, *95*, 6361.
(108) Garde, S.; Yang, L.; Dordick, J. S.; Paulaitis, M. E. *Mol. Phys.* **2002**, *100*, 2299.
(109) Edholm, O.; Berendsen, H. J. C.; van der Ploeg, P. *Mol. Phys.* **1983**, *48*, 379.
(110) Gruen, D. W. R. *J. Phys. Chem.* **1985**, *89*, 146.
(111) Gruen, D. W. R. *J. Phys. Chem.* **1985**, *89*, 153.
(112) Gruen, D. W. R. *Chem. Phys. Lipids* **1982**, *30*, 105.
(113) McMullen, W. E.; Gelbart, W. M.; Ben-Shaul, A. *J. Phys. Chem.* **1994**, *98*, 712.
(114) Dill, K. A. *Adv. Colloid Interface Sci.* **1986**, *26*, 99.
(115) Puvvada, S.; Blankschtein, D. *J. Phys. Chem.* **1992**, *96*, 5579.
(116) Huibers, P. D. T.; Lobanov, V. S.; Katritzky, A. R.; Shah, D. O.; Karelson, M. *Langmuir* **1996**, *12*, 1462.
(117) Hatton, T. A.; Nelson, P. H.; Rutledge, G. C. *J. Chem. Phys.* **1997**, *107*, 10777.
(118) Lah, J.; Pohar, C.; Vesnaver, G. *J. Phys. Chem. B* **2000**, *104*, 2522.

(119) Ladbury, J. E.; Chowdhry, B. Z. *Biocalorimetry: Applications of Calorimetry in the Biological Sciences*; John Wiley & Sons: Chichester, UK, 1998.
(120) Hubbard, S. J.; Thornton, J. M. *NACCESS*; University College London, 1993.
(121) Tsodikov, O. V.; Record, M. T.; Sergeev, Y. V. *J. Comput. Chem.* **2002**, *23*, 600.
(122) Stabinger, H.; Kratky, O. *Makromol. Chem.* **1978**, *179*, 1655.
(123) Glatter, O. *J. Appl. Crystallogr.* **1979**, *12*, 166.
(124) Glatter, O. *Acta Phys. Aust.* **1977**, *47*, 83.
(125) Glatter, O. *J. Appl. Crystallogr.* **1977**, *10*, 412.
(126) Glatter, O. Fourier Transformation and Deconvolution. In *Neutron, X-rays and Light: Scattering Methods Applied to Soft Condensed Matter*; Lindner, P., Zemb, T., Eds.; Elsevier: North-Holland, Amsterdam, 2002.
(127) Glatter, O. *J. Appl. Crystallogr.* **1981**, *14*, 101.
(128) Glatter, O.; Hainisch, B. *J. Appl. Crystallogr.* **1984**, *17*, 435.
(129) Mittelbach, R.; Glatter, O. *J. Appl. Crystallogr.* **1998**, *31*, 600
(130) Privalov, P. L.; Pothekin, S. A. *Methods Enzymol.* **1986**, *131*, 4.
(131) Freire, E. *Comments Mol. Cell. Biophys.* **1989**, *6*, 123.
(132) Freire, E.; Biltonen, R. L. *Biopolymers* **1978**, *17*, 463.
(133) Press, W. H.; Flannery, B. P.; Teukolsky, S. A.; Vetterling, W. T. *Numerical Recipes*; Cambridge University Press: Oxford, UK, 1992; p 650.
(134) Baldwin, L. R. *Proc. Natl. Acad. Sci. U.S.A.* **1986**, *83*, 8069.
(135) Lah, J.; Simic, M.; Vesnaver, G.; Marianovsky, I.; Glaser, G.; Engelberg-Kulka, H.; Loris, R. *J. Biol. Chem.* **2005**, *280*, 17397.
(136) Lah, J.; Prislan, I.; Kržan, B.; Salobir, M.; Francky, A.; Vesnaver, G. *Biochemistry* **2005**, *44*, 13883.
(137) Chan, H. S.; Dill, K. A. *J. Chem. Phys.* **1994**, *101*, 7007.
(138) Sharp, K. A.; Nicholls, A.; Friedman, R.; Honig, B. *Biochemistry* **1991**, *30*, 9686.
(139) Olofsson, G. *J. Phys. Chem.* **1985**, *89*, 1473.
(140) Andersson, B.; Olofsson, G. *J. Chem. Soc., Faraday Trans. 1* **1988**, *84*, 4087.
(141) Andersson, B.; Olofsson, G. *J. Solution Chem.* **1989**, *18*, 1019.
(142) Ohta, A.; Murakami, R.; Takiue, T.; Ikeda, N.; Aratono, M. *J. Phys. Chem. B* **2000**, *104*, 8592.
(143) Ohta, A.; Takiue, T.; Ikeda, N.; Aratono, M. *J. Solution Chem.* **2001**, *30*, 335.
(144) Weyerich, B.; Brunner-Popela, J.; Glatter O. *J. Appl. Crystallogr.* **1999**, *32*, 197.
(145) Tomšič, M.; Bešter-Rogač, M.; Jamnik, A.; Kunz, W.; Tourand, D.; Bergmann, A.; Glatter, O. *J. Phys. Chem. B* **2004**, *108*, 7021.
(146) Durchschlag, H.; Zipper, P. *Prog. Colloid Polym. Sci.* **1994**, *94*, 20.
(147) Durchschlag, H.; Zipper, P. *Jorn. Com. Esp. Deterg.* **1995**, *26*, 275.
(148) Finkelstein, A. V.; Janin, J. *Protein Eng.* **1989**, *3*, 1−3.
(149) Janin, J.; Chothia, C. *Biochemistry* **1978**, *17*, 2943.
(150) Lah, J.; Vesnaver, G. *J. Mol. Biol.* **2004**, *342*, 73.
(151) Rentzeperis, D.; Marky, L. A.; Dwyer, T. J.; Geierstanger, B. H.; Pelton, J. G.; Wemmer, D. E. *Biochemistry* **1995**, *34*, 2937.
(152) Chaires, J. B. *Biopolymers* **1997**, *44*, 201.
(153) Chaires, J. B. *Curr. Opin. Struct. Biol.* **1998**, *8*, 314.
(154) Haq, I.; Ladbury, J. E.; Chowdhry, B. Z.; Ren, J.; Chaires, J. B. *Methods Enzymol.* **1997**, *271*, 244.
(155) Dill, K. A.; Truskett, T. M.; Vlachy, V.; Hribar-Lee, B. *Annu. Rev. Biophys. Biomol. Struct.* **2005**, *34*, 173.
(156) Dill, K. A. *J. Biol. Chem.* **1997**, *272*, 701.